

# Broadband Macromodels for Retarded Partial Element Equivalent Circuit (rPEEC) Method

Giulio Antonini, *Member, IEEE*, Dirk Deschrijver, and Tom Dhaene, *Senior Member, IEEE*

**Abstract**—The partial element equivalent circuit (PEEC) method is, nowadays, widely used in electromagnetic compatibility and signal integrity problems in both the time and frequency domains. Similar to other integral-equation-based techniques, its time domain implementation may suffer from late time instabilities, especially when considering delays  $[(Lp, P, R, \tau)\text{PEEC}]$  (rPEEC). The cause of the instabilities may be either the numerical technique used for the time integration or problems created by the discrete representation of the electromagnetic continuous problem. In this paper, we concentrate on the latter and show that frequency dispersion plays an important role and must be taken into account in order to preserve accuracy and mitigate instabilities issues. An enhanced formulation of the PEEC method is presented that is based on a more accurate computation of partial elements describing the electric and magnetic field couplings; broadband macromodels are generated incorporating the frequency dependence of such elements, thus, allowing us to obtain better stability properties of the resulting  $(Lp, P, R, \tau)\text{PEEC}$  model. The proposed equivalent circuits resemble those of the standard PEEC formulation but are able to capture the dispersion that, when neglected, might contribute to inaccuracies and late time instabilities.

**Index Terms**—Broadband macromodels for retarded partial element equivalent circuit (rPEEC) method, transient analysis.

## I. INTRODUCTION

WITH the increasing need to analyze wide frequency band electrical problems, accurate numerical modeling has become a challenging task as typical high-frequency phenomena such as skin effect and dielectric losses must be taken into account. These effects are quite easily modeled by using a frequency domain approach based on frequency-dependent constitutive parameters. Nevertheless, time domain solvers are becoming increasingly more popular because they are often faster than their frequency domain counterparts, they can gather broadband data in a single simulation, and they can model time-varying and nonlinear scattering-radiation problems. Furthermore, if appropriate techniques are used, their complexity can be nearly  $O(N)$  [1]. Over the years, many different time domain techniques have been developed such as the finite-difference time domain (FDTD) method [2], [3], the time domain finite element (TD-FE) method [4], or the time domain integral equations (TDIEs) method [5]. In the class of TDIE methods, the computational efficiency has been

greatly improved by the advent of fast solution schemes based on the fast multipole technique [6], [7], the plane wave time domain, and the hierarchical fast fourier transform (FFT) methods [8]–[11]. More recently, an interesting numerically stable broadband electromagnetic solver based on the adaptive integral method (AIM) has been presented [12]. The recent advances in TDIE research has allowed TDIE-based solvers to compete with more mature methods such as FDTD and TD-FE.

Among the integral-equation-based methods, the partial element equivalent circuit (PEEC) method [13]–[15] has received great attention for its capability to deal with mixed electromagnetic and circuit problems. In the recent past, much progress has been made in improving the versatility of the method. In particular, it has been recently extended to nonorthogonal structures [16], more advanced skin effect models have been proposed [17], and lossy and dispersive dielectrics have been modeled as well [18]. It is to be mentioned that the PEEC method models the electric and magnetic field couplings correctly, precluding the low-frequency breakdown that plagues the standard method-of-moments-based techniques and requires special bases in order to capture the low-frequency physics [19].

Despite this progress, the issue of the stability of the method is still open and, analogously to other TDIE methods, hampers its robust use for developing efficient time domain solvers. The stability of PEEC models has been studied in several papers. In [20], the authors focus on the impact of the numerical methods used to integrate the delay differential equations (DDEs) of PEEC circuits on their stability. It is known that a good numerical integration rule is not enough to ensure the stability as the model itself may not be stable due to poor modeling or computation of coupling coefficients. In [21], a splitting current cell procedure is proposed in order to improve the stability properties of the resulting circuit; an even more significant improvement of stability can be achieved by adding additional damping resistances in parallel to self-inductances. Although the last two papers improve the stability properties of PEEC circuits, they do not solve all the instability issues as they do not tackle the root cause of the problem.

More recently, the stability of full-wave PEEC models has been investigated [22], [23], and an improved PEEC model has been proposed, providing better performance with respect to stability. In the cited papers, for the first time, it has been pointed out that instability and inaccuracy are related to poor approximation of double integrals over the complex Green's function. Nevertheless, the approach proposed in [22] and [23] is based on a predefined model that presents the following limits: 1) It only uses coincident real poles to reproduce the damping observed in partial elements, which is quite limiting,

Manuscript received October 13, 2005; revised September 12, 2006.

G. Antonini is with Electromagnetic Compatibility Research Laboratory, Department of Electrical Engineering, University of L'Aquila, 67040 L'Aquila, Italy (e-mail: antonini@ing.univaq.it).

D. Deschrijver and T. Dhaene are with the Computer Modeling and Simulation (COMS) Group, University of Antwerp, B-2020, Antwerp, Belgium (e-mail: dirk.deschrijver@ua.ac.be; tom.dhaene@ua.ac.be).

Digital Object Identifier 10.1109/TEMC.2007.888170

and 2) nowadays, in complex structures, the location of poles may extend up to 1000 GHz, still having an impact in the low-frequency range; in the authors' experience, the proposed predefined function may require very high orders to preserve accuracy and stability, which leads to a significant increase of the computational complexity.

In this paper, the frequency dependence of partial elements is investigated, namely partial inductances and coefficients of potential, which describe the magnetic and electric field coupling, respectively, and macromodels are proposed to capture the physics of the frequency-dependent couplings. Furthermore, a new orthonormal vector fitting (OVF) algorithm [24], [25] is adopted to build pole-residue macromodels; this significantly reduces the numerical sensitivity of the model parameterization to the choice of starting poles and limits the number of required pole relocation iterations. The final macromodel is, basically, a simplified terminal model that allows the analysis of systems that exhibit complex frequency behavior. It is also worth noting that a wideband frequency domain analysis cannot leave aside the frequency dependence of partial elements and that the subsequent fitting adds only a minimum amount of workload.

The enhanced PEEC time domain solver proposed in this work is based on a two-step procedure: 1) delay extraction and 2) OVF approximation of delayless terms.

The final target of this work is to provide a new broadband PEEC discrete model that is accurate from dc up to a maximum frequency of interest, thus being suitable for ultra-wide band applications. The proposed technique does not aim to extract poles of the PEEC continuous system; the interested reader may want to refer to [26] and [27], where a pole-residue approximation of PEEC systems is presented, taking into account a center-to-center representation of delays.

The paper is organized as follows. Section III details the frequency dependence of partial elements and the formulation for the delay extraction and rational approximation; in Section IV, the OVF algorithm is presented; Section V presents the circuit synthesis of macromodels described in Section III; Section VI is devoted to present the implementation of the time domain PEEC (TD-PEEC) solver; numerical results that support the accuracy and stability claims of Section V are presented in Section VII. Finally, Section VIII provides conclusions and suggestions for future improvements.

## II. PEEC FORMULATION

The PEEC method is derived by summing all sources of electric field inside a conductor

$$\mathbf{E}^{\text{ext}}(\mathbf{r}, s) = \frac{\mathbf{J}(\mathbf{r}, s)}{\gamma} + s\mathbf{A}(\mathbf{r}, s) + \nabla V(\mathbf{r}, s) \quad (1)$$

where  $\mathbf{E}^{\text{ext}}$  represents an applied field. The vector and scalar potentials  $\mathbf{A}$  and  $V$ , respectively, are expressed in terms of integrals

$$\mathbf{A}(\mathbf{r}, s) = \sum_{k=1}^K \frac{\mu}{4\pi} \int_{V_k} \frac{e^{-s|\mathbf{r}-\mathbf{r}'|/c_0}}{|\mathbf{r}-\mathbf{r}'|} \mathbf{J}(\mathbf{r}', s) dv' \quad (2)$$

and

$$V(\mathbf{r}, s) = \sum_{k=1}^K \frac{1}{4\pi\epsilon} \int_{S_k} \frac{e^{-s|\mathbf{r}-\mathbf{r}'|/c_0}}{|\mathbf{r}-\mathbf{r}'|} q(\mathbf{r}', s) dS' \quad (3)$$

where  $K$  is the number of conductors involved, and  $\mathbf{J}$  and  $q$  are the current and charge density, respectively. Its extension to include dielectrics is straightforward [28] and is not presented here.

In [13] and [14], it is shown that through Galerkin's approach, it is possible to give a circuit interpretation to (1): More specifically, (2) leads to the concept of partial inductances of the form

$$L_{p,mn}(s) = \frac{\mu}{4\pi a_m a_n} \int_{v_m} \int_{v_n} \frac{e^{-s|\mathbf{r}_m-\mathbf{r}_n|/c_0}}{|\mathbf{r}_m-\mathbf{r}_n|} dv_m dv_n \quad (4)$$

for two hexahedral volumes  $m$  and  $n$  with cross sections  $a_m$  and  $a_n$ , while (3) allows us to obtain the coefficient of potential given by

$$P_{mn}(s) = \frac{1}{4\pi\epsilon S_m S_n} \int_{S_m} \int_{S_n} \frac{e^{-s|\mathbf{r}_m-\mathbf{r}_n|/c_0}}{|\mathbf{r}_m-\mathbf{r}_n|} dS_m dS_n \quad (5)$$

for two patches  $m$  and  $n$  with surfaces  $S_m$  and  $S_n$ , assuming that charge is only located on the surface of conductors. This paper focuses on the construction of broadband macromodels of (4) and (5) to be used into a PEEC simulator such that the frequency dependence is correctly exploited.

## III. FREQUENCY-DEPENDENT PARTIAL ELEMENTS

This section focuses on the frequency dependence of PEEC partial elements, namely partial inductances and coefficients of potential; more specifically, Section III-A discusses the derivation of a macromodel for magnetic field coupling involving double folded volume integrals; Section III-B describes the same macromodeling generation for the electric field coupling that involves double folded surface integrals.

### A. Partial Inductances

As previously stated, the magnetic field coupling between volume cells  $m$  and  $n$  is described in terms of the complex partial inductance

$$L_{p,mn}(s) = \frac{\mu}{4\pi a_m a_n} \int_{v_m} \int_{v_n} \frac{e^{-s|\mathbf{r}_m-\mathbf{r}_n|/c_0}}{|\mathbf{r}_m-\mathbf{r}_n|} dv_m dv_n \quad (6)$$

where  $c_0$  is the free-space speed of light, and  $a_m$  and  $a_n$  are the cross sections of volume cells  $m$  and  $n$ . In TD-PEEC modeling, it is a common practice to assume a center-to-center approximation for the exponential term that can be taken out of the integral yielding

$$L_{p,mn}(s) = e^{-s\tau_{mn}^L} L_{p,mn}^{\text{st}} \quad (7)$$

where  $\tau_{mn}^L = R/c_0$  is the center-to-center fly time between cells  $m$  and  $n$ ,  $R$  is the center-to-center distance between the cells, and the static mutual partial inductance is defined as

$$L_{p,mn}^{\text{st}} = \frac{\mu}{4\pi a_m a_n} \int_{v_m} \int_{v_n} \frac{1}{|\mathbf{r}_m-\mathbf{r}_n|} dv_m dv_n. \quad (8)$$

Volume integrals (6)–(8) can be evaluated by using numerical methods [29] or closed formulas [30], [31]. Also, advanced techniques can be used to speed up their computation [32], [33].

The standard delay extraction assumes that the delayless part is no longer frequency-dependent. This assumption implies a

limited and, thus, acceptable loss of accuracy for electrically small structures but may cause significant errors in the case of electrically large objects whose dimensions exceed  $\lambda_{\min}$ , corresponding to the maximum frequency of interest. For these kinds of problems, a more rigorous technique is required to properly model the frequency dependence of partial elements. As pointed out in [34], the direct rational approximation of partial inductances and coefficients of potential over a broad frequency band is a difficult task because of the exponential term in (7). It generates two different classes of phenomena: First, the time delay of the electromagnetic fields that propagate from the source to the observation point causes fast variations in phase; second, the dispersion [35] causes slow variations in magnitude. These kinds of problems are usually mitigated by using delay extraction.

Typically, delay extraction is used in the method of characteristics [34], [36], [37] while studying long transmission lines. Interesting examples of delay extraction for transmission lines can be found in [34] and [37]. In the PEEC framework, all the electric as well as magnetic field couplings are established in air since dielectric polarization currents are modeled locally by excess capacitances. This allows an easy and reasonable estimate of the delay as the center-to-center time-of-flight, as in (7). Nevertheless, the approximation (7) may be significantly wrong for electrically large structures because of dispersive effects, which still affects the delayless part. Thus, a better and more accurate model is required.

As previously stated, the time delay for the electromagnetic field to propagate from cell  $n$  to cell  $m$  can be approximated as  $\tau_{mn}^L = R/c_0$ , where  $R$  is the center-to-center distance. This task allows to write the complex impedance  $Z_{L,mn}(s)$  as

$$Z_{L,mn}(s) = sL_{p,mn}(s) = Z_{L,mn}^{\text{dl}}(s)e^{-s\tau_{mn}^L} \quad (9)$$

where the delayless impedance  $Z_{L,mn}^{\text{dl}} = sL_{p,mn}(s)e^{s\tau_{mn}^L}$  is still frequency-dependent and takes dispersive phenomena into account at very high frequencies. The branch voltage induced on volume cell  $m$  due to the current flowing in volume cell  $n$  reads

$$V_{b,mn}(s) = Z_{L,mn}^{\text{dl}}(s)I_{L,n}(s)e^{-s\tau_{mn}^L}. \quad (10)$$

Typically, the computation of its time domain counterpart can be performed by

- a) standard convolution techniques;
- b) recursive convolution techniques via rational approximation of  $Z_{L,mn}^{\text{dl}}(s)$ .

Recursive convolution techniques can significantly speed up the convolution process but are not easily incorporated into a simulation program with integrated circuit emphasis (SPICE)-like solver based on the PEEC method, which is clearly circuit-oriented. An alternative approach is based on the circuit synthesis of  $Z_{L,mn}^{\text{dl}}(s)$  once the rational approximation model has been built. In fact, function  $Z_{L,mn}^{\text{dl}}(s)$  can be represented by Foster's canonical form and fitted by using standard frequency

domain techniques [38], [39], yielding

$$Z_{L,mn}^{\text{dl}}(s) = d_{mn}^L + se_{mn}^L + \sum_{k=1}^{N_p^r} \frac{\text{Res}_k^r}{s - p_k^r} + \sum_{k=1}^{N_p^c} \left( \frac{\text{Res}_k^c}{s - p_k^c} + \frac{\text{Res}_k^{c*}}{s - p_k^{c*}} \right) \quad (11)$$

where  $\text{Res}_k^r$ ,  $p_k^r$ , and  $N_p^r$  refer to real poles,  $\text{Res}_k^c$ ,  $p_k^c$ , and  $N_p^c$  are the same quantities for the complex conjugate pairs, and  $*$  denotes the complex conjugate operator. In Section V, a short overview of circuit synthesis techniques will be given to model (11).

### B. Coefficients of Potential

The electric field coupling is described by a complex coefficient of potential. Considering two cells  $m$  and  $n$ , the mutual coefficient of potential is

$$P_{mn}(s) = \frac{1}{4\pi\epsilon S_m S_n} \int_{S_m} \int_{S_n} \frac{e^{-s|\mathbf{r}_m - \mathbf{r}_n|/c_0}}{|\mathbf{r}_m - \mathbf{r}_n|} dS_m dS_n \quad (12)$$

where  $S_m$  and  $S_n$  represent the area of surface cells  $m$  and  $n$ . The enhanced model for capacitive coupling can be obtained in a similar way, as described in Section III-A. In the standard PEEC modeling, the center-to-center approximation is used, and the complex coefficient of potential is approximated as

$$P_{mn}(s) = e^{-s\tau_{mn}^C} P_{mn}^{\text{st}} \quad (13)$$

where  $P_{mn}^{\text{st}}$  is assumed to be frequency-independent. As in the case of magnetic field coupling, this assumption may cause significant inaccuracies, and the use of a frequency-dependent remaining part may be advised. Usually, two different approaches are used to synthesize equivalent circuit describing the electric field coupling; the first one uses impedances, which are synthesized by voltage-controlled voltage sources (VCVSs); the second one uses admittances and, correspondingly, current-controlled current sources (CCCSs). In the following paragraphs, the first approach will be discussed.

The impedance describing mutual electric field coupling is given by

$$Z_{C,mn}(s) = \frac{P_{mn}(s)}{s}. \quad (14)$$

The center-to-center delay  $\tau_{mn}$  can be extracted so that

$$Z_{C,mn}(s) = Z_{C,mn}^{\text{dl}}(s) e^{-s\tau_{mn}^C} \quad (15)$$

where  $Z_{C,mn}^{\text{dl}}(s)$  is the delayless impedance given by

$$Z_{C,mn}^{\text{dl}}(s) = Z_{C,mn}(s) e^{s\tau_{mn}^C}. \quad (16)$$

The pole-residue representation of  $Z_{C,mn}(s)$  leads to

$$Z_{C,mn}^{\text{dl}}(s) = d_{mn}^C + se_{mn}^C + \sum_{k=1}^{N_p^r} \frac{\text{Res}_k^r}{s - p_k^r} + \sum_{k=1}^{N_p^c} \left( \frac{\text{Res}_k^c}{s - p_k^c} + \frac{\text{Res}_k^{c*}}{s - p_k^{c*}} \right) \quad (17)$$

where, as before,  $\text{Res}_k^r, p_k^r$ , and  $N_p^r$  refer to real poles, and  $\text{Res}_k^c, p_k^c$ , and  $N_p^c$  are the same quantities for the complex conjugate pairs. The impedance formulation has a pole at zero, and this may cause problems when solving the overall system of DDEs, as will be shown in Section VI-C. This issue can be overcome by slightly moving the pole at zero to the left-half complex plane by a small amount, typically of the order of the precision machine ( $10^{-16}$ ); in this way, the procedure outlined in this section can be adopted with no change.

It is also worth noting that the additional workload to build the rational approximations of partial elements, as described in Section VI, is significantly reduced due to upfront delay extraction. Thus, in the authors' experience, the CPU time required to build the broadband rational approximation of partial elements is comparable with the computation of one single frequency sample.

#### IV. OVF

The major goal of the identification process is to characterize the delayless terms (11) and (17) by a rational analytic model. For continuous-time linear, time-invariant (LTI) systems in the frequency domain, this reduces to approximating the system parameters of the transfer function in a reliable and computationally efficient way. It is well known that this identification problem is numerically hard to solve, especially for broadband frequency domain responses of highly dynamical systems. Recently, a new identification algorithm called OVF [24], [25] was proposed, which accurately approximates the impedance data ( $s_w, Z_{L, mn}^{\text{dl}}(s_w)$  or  $Z_{C, mn}^{\text{dl}}(s_w)$ ) at multiple complex frequencies  $s_w$ , for  $w = 0, \dots, W$ , by estimating the model parameters of a rational function  $R(s)$ . Such a rational function can be represented in Foster's canonical form, as shown in (11) and (17). In order to estimate the unknown poles  $p_k$  and residues  $\text{Res}_k$ , the transfer function is represented as follows:

$$\begin{aligned} R(s) &= \frac{N(s)}{D(s)} \\ &= \frac{\sum_{k=1}^{N_p^r} \widetilde{\text{Res}}_k^r \phi_k^r(s) + \sum_{k=1}^{N_p^c} \widetilde{\text{Res}}_k^c \phi_k^c(s) + d + se}{\sum_{k=1}^{N_p^r} \widetilde{\text{Res}}_k^r \phi_k^r(s) + \sum_{k=1}^{N_p^c} \widetilde{\text{Res}}_k^c \phi_k^c(s) + \widetilde{\text{Res}}_0}. \end{aligned} \quad (18)$$

Here, an optional constant ( $d$ ) and an optional linear term ( $se$ ) can be added to the numerator expression in order to make the transfer function  $R(s)$  a proper or an improper rational function, respectively. The OVF method is essentially based on the vector fitting (VF) routine of Gustavsen and Semlyen [38], which uses partial fractions as a rational basis but has improved numerical properties. Due to the orthonormality of the new basis functions, the identification of poles and residues is, often, significantly better conditioned, especially if the real part of the (starting) poles is nonnegligible. So, accurate fitting models can usually be obtained in fewer iterations, which reduces the overall computation time [40].

#### A. Choice of Basis Functions

It is noted that both the numerator and denominator are expanded in a common set of rational basis functions  $\phi_k(s)$ , which are orthonormal

$$\langle \phi_m(s), \phi_n(s) \rangle = \delta_{mn} \quad (19)$$

for  $1 < m, n < N_p$ , with respect to the continuous inner product

$$\langle \phi_m(s), \phi_n(s) \rangle = \frac{1}{2\pi i} \int_{\mathbb{R}} \phi_m(s) \phi_n^*(s) ds. \quad (20)$$

The orthonormal basis can be calculated easily by applying a Gram-Schmidt orthonormalization on a set of partial fractions, which leads to the following closed-form expression:

$$\phi_k^r(s) = \frac{\sqrt{-2\Re(p_k)}}{(s - p_k)} \left( \prod_{j=1}^{k-1} \frac{s + p_j^*}{s - p_j} \right). \quad (21)$$

Remark, however, that these basis functions (21) are not real-valued by construction. To avoid imaginary terms in the time domain, it is desired that the polynomial coefficients of the numerator and denominator are real, such that  $R^*(s) = R(s^*)$ . The fitting algorithm ensures that this property is satisfied by making the basis functions real-valued and their corresponding coefficients real. If the basis functions  $\phi_k^c(s)$  and  $\phi_{k+1}^c(s)$  correspond to a complex conjugate pair of poles  $p_k^* = p_{k+1}^c$ , a linear combination is formed

$$\phi_k^c(s) = \frac{\sqrt{-2\Re(p_k^c)}(s - |p_k^c|)}{(s - p_k^c)(s - p_k^{c*})} \left( \prod_{j=1}^{k-1} \frac{s + p_j^*}{s - p_j} \right) \quad (22)$$

$$\phi_{k+1}^c(s) = \frac{\sqrt{-2\Re(p_k^c)}(s + |p_k^c|)}{(s - p_k^c)(s - p_k^{c*})} \left( \prod_{j=1}^{k-1} \frac{s + p_j^*}{s - p_j} \right). \quad (23)$$

#### B. Pole Identification and Relocation

The goal of the identification problem is to find the optimal values of the indeterminates  $v = \{\widetilde{\text{Res}}_k^r, \widetilde{\text{Res}}_k^c, \widetilde{\text{Res}}_k, \widetilde{\text{Res}}_0, d, e\}$  and  $p = \{p_k^r, p_k^c\}$ , such that the following nonlinear cost function is minimized in a fast and computationally efficient way:

$$\arg \min_{v, p} \sum_{w=0}^W \left| \frac{N(s_w)}{D(s_w)} - Z(s_w) \right|^2. \quad (24)$$

Based on a set of prescribed poles  $p$ , the remaining unknowns  $v$  can be estimated by minimizing Levi's cost function [41] ( $\widetilde{\text{Res}}_0 = 0$ )

$$\arg \min_v \sum_{w=0}^W |N(s_w) - D(s_w)Z(s_w)|^2 \quad (25)$$

where  $N(s_w)$  and  $D(s_w)$  are defined as in (18). It is clear that the transfer function can be simplified by canceling out the common poles. The consequence of this operation is that the poles of the simplified transfer function become equal to the zeros of  $D(s)$ . These zeros can be calculated accurately by

constructing its minimal state–space realization and by solving an eigenvalue problem. For details, see [25] and [42]. Based on the calculated poles, this procedure can be repeated in an iterative fashion. It can be shown that this iterative procedure basically reduces to the Sanathanan–Koerner (SK) iteration.

Note that the SK iteration is not equivalent to a nonlinear cost function and that convergence to the true fundamental solution of the least-squares problem is not necessarily guaranteed. In practice, however, the solutions are often sufficiently accurate for high signal-to-noise ratios. If not, they can often provide good starting points for nonlinear optimization techniques.

Once the poles are estimated, the transfer function can be represented as a linear combination of partial fractions (i.e., Foster’s canonical form), as shown in (11) and (17). The calculation of the residues becomes a linear problem, which can be solved easily.

Although the proposed method improves the stability properties of the PEEC method, as it allows to model the damping of partial elements, it is known that passivity of the equivalent circuits model can still be violated, thus leading to instabilities in time domain. Recently, passivity enforcement techniques have been proposed [43], [44] and applied to problems with a reduced number of unknowns, as a postprocessing process. For large problems with thousands of unknowns and delays, as those arising in PEEC modeling, passivity enforcement is a challenging task that deserves a systematic approach; a more quantitative analysis of the passivity of retarded PEEC (rPEEC) models will be investigated and reported in the forthcoming papers.

## V. ENHANCED EQUIVALENT CIRCUIT SYNTHESIS

This section details the procedure that allows to build enhanced equivalent circuits taking into account the frequency dependence of partial elements to be used into a modified nodal analysis (MNA) based solver [45].

### A. Impedance Synthesis

In the following paragraphs, the suffixes  $L$  and  $C$  are omitted for brevity, and synthesis refers to both  $Z_{L,mn}(s)$  and  $Z_{C,mn}(s)$ .

The constant term  $d$  corresponds to an additional resistance  $R_{\text{add}}$  taking into account the losses due to magnetic and electric mutual coupling:

$$R_{\text{add}} = d. \quad (26)$$

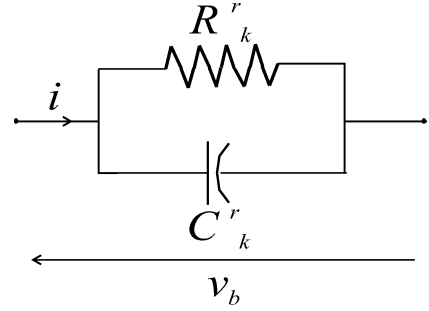


Fig. 1. Equivalent circuit for real poles.

The proportional term is directly modeled as an inductance  $L_0$

$$L_0 = e. \quad (27)$$

The  $k$ th residue and pole can be synthesized easily by means of an  $RC$  parallel equivalent circuit, as shown in Fig. 1. The values of the equivalent circuit parameters are

$$C_k^r = 1/\text{Res}_k^r \quad (28)$$

$$R_k^r = -\frac{\text{Res}_k^r}{p_k^r}. \quad (29)$$

Any discretization scheme can be used to model the previous circuit into a time discrete solver, leading to the circuit shown in Fig. 2. If the simple backward Euler (BE) scheme is adopted and a time discretization is assumed, the values of parameters are

$$G_{\text{eq}}^r = \left( \frac{1}{R_k^r} + \frac{C_k^r}{dt} \right) \quad (30)$$

$$i_{s,\text{eq}}(n-1) = \frac{C_k^r}{dt} v_b(n-1) \quad (31)$$

which results into the following time discrete equation:

$$i(n) = G_{\text{eq}} v_b(n) - i_{s,\text{eq}}(n-1). \quad (32)$$

In the case of complex conjugate pair, the  $k$ th residue and pole, along with their conjugate counter part, are synthesized by using an  $RLCG$  equivalent circuit [46], as shown in Fig. 3. The values of parameters for a complex pole pair are as in (33), shown at the bottom of the page, where  $*$  denotes the complex conjugate operator. The same time discrete circuit in Fig. 2 can be used to implement the equivalent circuit into a time discrete

$$\begin{aligned} C_k^c &= \frac{1}{\text{Res}_k + \text{Res}_k^*} \\ G_{2k}^c &= \frac{1}{\text{Res}_k + \text{Res}_k^*} - (p_k + p_k^*) + \frac{\text{Res}_k p_k^* + \text{Res}_k^* p_k}{\text{Res}_k + \text{Res}_k^*} \\ L_k^c &= \frac{\text{Res}_k + \text{Res}_k^*}{[p_k p_k^* + \{(p_k + p_k^*) + (\text{Res}_k p_k^* + \text{Res}_k^* p_k)/(\text{Res}_k + \text{Res}_k^*)\}](\text{Res}_k p_k^* + \text{Res}_k^* p_k)/(\text{Res}_k + \text{Res}_k^*)} \\ G_{1k}^c &= -\frac{(\text{Res}_k p_k^* + \text{Res}_k^* p_k)(\text{Res}_k + \text{Res}_k^*)}{L_k^c} \end{aligned} \quad (33)$$

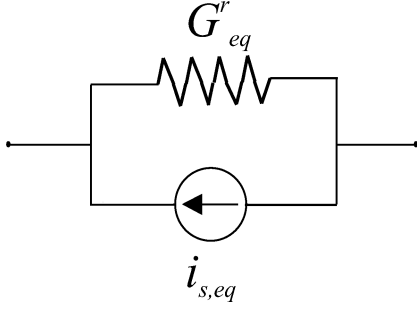


Fig. 2. Time discrete equivalent circuit.

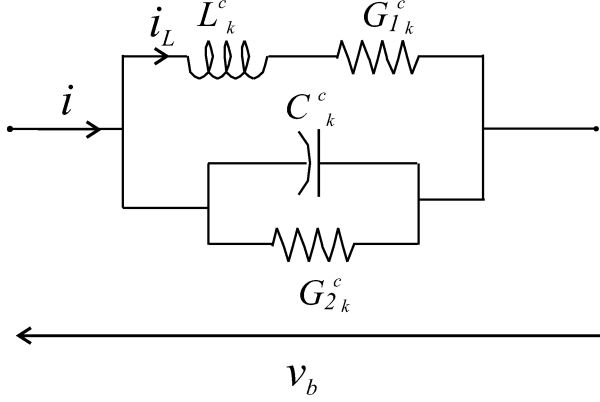


Fig. 3. Equivalent circuit for a complex poles pair solver. In the this case, the MNA stamps are

$$G^c_{eq} = \left( \frac{1}{G^c_{1k}} + \frac{L^c_k}{dt} \right)^{-1} + \left( G^c_{2k} + \frac{C^c_k}{dt} \right) \quad (34)$$

$$i^c_{s,eq}(n) = - \left( \frac{1}{G^c_{1k}} + \frac{L^c_k}{dt} \right)^{-1} \frac{L^c_k}{dt} i_L(n-1) + \frac{C^c_k}{dt} v_b(n-1). \quad (35)$$

Obviously, the time discrete equivalent circuit has the same topology as the one in Fig. 2. It is to be pointed out that the equivalent circuit synthesizing the magnetic and electric field couplings between cells  $m$  and  $n$  represents an improvement of the standard rPEEC models. In fact, the standard rPEEC method [20], [21] considers only the static part of  $Z_{L,mn}(s)$  and  $Z_{C,mn}(s)$ , while the proposed ones are able to take into account the dispersive and lossy behavior.

In [47], additional losses have been arbitrarily added as additional resistances in parallel to self-inductances in order to improve the stability of PEEC models. They have a positive impact on stability, but at the same time, they may significantly affect the accuracy of the results as they do not have any clear physical meaning. However, the proposed method is physically consistent as resistances  $R_k$  and conductances  $G^c_{1k}$  are effective only at higher frequencies, when dispersive effects are more pronounced. It may be argued that such macromodel generation can be time-consuming when applied to a large number of partial elements because, for each of them, it needs 1) the computation over a wide frequency range and 2) the rational approximation (11) and (17). These requirements are significantly alleviated

by the delay extraction because delayless impedances (11) and (17) are characterized by slow variations in magnitude and limited variations of phase. This allows the use of a limited number of frequency samples and poles (usually zero to five poles are sufficient to capture the broadband delayless impedances behavior).

## VI. TIME DOMAIN IMPLEMENTATION

### A. Magnetic Field Coupling

The branch voltage induced on volume  $m$  due to currents flowing in the volume cells, in the Laplace domain, is given by

$$V_{b,m}(s) = \sum_{n=1}^{N_L} V_{b,mn}(s) = \sum_{n=1}^{N_L} [Z_{L,mn}(s)I_{L,n}(s)] + V_{s,m}^{\text{ext}}(s) \quad (36)$$

where  $N_L$  is the number of inductive cells, and  $V_{s,m}^{\text{ext}}$  represents a voltage source due to an external field coupling [48].  $Z_{L,mn}(s)$  is assumed to be expanded as in (9) for the mutual case  $m \neq n$ , while the quasi-static approach  $Z_{L,mn}(s) = sL_{p,mm}$  is used for the self-case  $m = n$ .

The voltage induced on cell  $m$  by current flowing in cell  $n$  can be mapped into a time discrete form that, assuming a time step  $h$  at time  $t = kh$ , reads

$$v_{b,mn}(k) = d_{mn}^L i_n(k - \tau_{h,mn}^L) + \frac{e_{mn}^L}{dt} [i_{L,n}(k - \tau_{h,mn}^L) - i_{L,n}(k-1 - \tau_{h,mn}^L)] + \left[ \sum_{i=1}^{N_r} \frac{1}{G^r_{eq,i}} + \sum_{i=1}^{N_c/2} \frac{1}{G^c_{eq,i}} \right] i_{L,n}(k - \tau_{h,mn}^L) + v_{s,mn}^{\text{eq}}(k-1 - \tau_{h,mn}^L) \quad (37)$$

$$= R_{eq,mn} i_{L,n}(k - \tau_{h,mn}^L) + v_{s,mn}^{\text{eq}}(k-1 - \tau_{h,mn}^L) \quad (38)$$

where  $\tau_{h,mn}^L = \tau_{mn}^L/dt$ ,  $dt$  being the time step, and

$$R_{eq,mn} = \sum_{i=1}^{N_r} \frac{1}{G^r_{eq,i}} + \sum_{i=1}^{N_c/2} \frac{1}{G^c_{eq,i}} + d_{mn}^L + \frac{e_{mn}^L}{dt} \quad (39)$$

$$v_{s,mn}^{\text{eq}}(k-1 - \tau_{h,mn}^L) = \sum_{i=1}^{N_r} \frac{1}{G^r_{eq,i} i^r_{s,eq}} (k-1 - \tau_{h,mn}^L) + \sum_{i=1}^{N_c/2} \frac{1}{G^c_{eq,i} i^c_{s,eq}} (k-1 - \tau_{h,mn}^L) - \frac{e_{mn}^L}{dt} i_n(k-1 - \tau_{h,mn}^L) \quad (40)$$

where  $N_r$  is the number of real poles, and  $N_c$  is the number of complex pairs used for fitting the delayless impedance  $Z_{L,mn}^{\text{dl}}(s)$ . The global voltage induced on the volume cell  $m$  is,

finally

$$v_{b,m}(k) = \sum_{n=1}^{N_L} v_{b,mn}(k) + v_{b,m}^{\text{ext}}(k). \quad (41)$$

In a matrix form, it becomes

$$\mathbf{v}_b(k) = \tilde{\mathbf{R}}_L \mathbf{i}_L(k - \tau_h^L) + \mathbf{\Psi}(k - 1 - \tau_h^L) + \mathbf{v}_S^{\text{ext}}(k) \quad (42)$$

where the  $m$ th entry of vector  $\mathbf{\Psi}(k - 1 - \tau_h^L)$  is

$$\Psi_m(k - 1 - \tau_h^L) = \sum_{n=1}^{N_L} v_{S,mn}^{\text{eq}}(k - 1 - \tau_{h,mn}^L). \quad (43)$$

Obviously, if any higher order discretization scheme [49] is used rather than BE, a similar equation is obtained involving multiple delay terms.

Branch voltages  $\mathbf{v}_b$  can be related to potentials to infinity  $\mathbf{v}$  by means of the connectivity matrix  $\mathbf{A}$

$$\mathbf{v}_b = -\mathbf{A}\mathbf{v} \quad (44)$$

where the connectivity matrix  $\mathbf{A}$  entries are

$$a_{ij} = \begin{cases} -1, & \text{if branch } i \text{ leaves node } j \\ 1, & \text{if branch } i \text{ enters node } j \\ 0, & \text{otherwise} \end{cases} \quad (45)$$

Thus, (41) can be rewritten as

$$-\mathbf{A}\mathbf{v}(k) - \tilde{\mathbf{R}}_L \mathbf{i}_L(k - \tau_h^L) = \mathbf{\Psi}(k - 1 - \tau_h^L) + \mathbf{v}_S^{\text{ext}}(k). \quad (46)$$

### B. Electric Field Coupling

Electric field coupling assumes infinity as the reference point. The potential induced on surface cell  $m$  by all the charges on the conductors is

$$V_m(s) = \sum_{n=1}^{N_c} Z_{C,mn}(s) I_{C,n}(s) \quad (47)$$

where  $V_m(s)$  is the potential to infinity of node  $m$ .  $Z_{C,mn}(s)$  is assumed to be expanded, as in (15). For the electric field coupling, there is no need to distinguish between self- and mutual cases because, as a consequence of the node-reduction process [50], all the coefficients have frequency-dependent magnitude. With all of the considerations done in the previous section, the potentials to infinity can finally be written as

$$\mathbf{v}(k) = \tilde{\mathbf{R}}_C \mathbf{i}_C(k - \tau_h^C) + \mathbf{\Phi}(k - 1 - \tau_h^C) \quad (48)$$

where  $\mathbf{\Phi}(k - 1 - \tau_h^C)$  is assembled as  $\mathbf{\Psi}(k - 1 - \tau_h^L)$  in Section VI-A.

Displacement currents, flowing from each node to infinity, can be expressed in terms of inductive currents  $\mathbf{i}_L$ , flowing into branches connecting couples of nodes, and lumped sources  $\mathbf{i}_S$  by means of Kirchhoff's current law (KCL) as

$$\mathbf{i}_C(k - \tau_h^C) = \mathbf{A}^T \mathbf{i}_L(k - \tau_h^C) + \mathbf{i}_S(k - \tau_h^C) \quad (49)$$

where  $\mathbf{A}$  is the connectivity matrix, and  $\mathbf{i}_S(k - \tau_h^C)$  represents the lumped current sources vector. Hence, (48) can be rewritten

as

$$\mathbf{v}(k) - \tilde{\mathbf{R}}_C \mathbf{A}^T \mathbf{i}_L(k - \tau_h^C) = \mathbf{\Phi}(k - 1 - \tau_h^C) + \tilde{\mathbf{R}}_C \mathbf{i}_S(k - \tau_h^C). \quad (50)$$

In order to make the MNA stamps more simple, it is more convenient to have (50) written in terms of current as

$$\tilde{\mathbf{R}}_C^{-1} \mathbf{v}(k) - \mathbf{A}^T \mathbf{i}_L(k - \tau_h^C) = \tilde{\mathbf{R}}_C^{-1} \mathbf{\Phi}(k - 1 - \tau_h^C) + \mathbf{i}_S(k - \tau_h^C). \quad (51)$$

### C. Advanced PEEC Solver

Any kind of PEEC solver is based on the enforcement of Kirchhoff's voltage law (KVL) to each fundamental loop and KCL to each node with the exception of the reference node at infinity. Equations (44) and (51) automatically imply KVL and KCL, respectively, and can be assumed as constituting the sets of algebraic delay equations (ADEs) to be solved at time step  $k$ :

$$\begin{cases} -\mathbf{A}\mathbf{v}(k) - \tilde{\mathbf{R}}_L \mathbf{i}_L(k - \tau_h^L) = \mathbf{\Psi}(k - 1 - \tau_h^L) + \mathbf{v}_S^{\text{ext}}(k) \\ \tilde{\mathbf{R}}_C^{-1} \mathbf{v}(k) - \mathbf{A}^T \mathbf{i}_L(k - \tau_h^C) = \tilde{\mathbf{R}}_C^{-1} \mathbf{\Phi}(k - 1 - \tau_h^C) + \mathbf{i}_S(k - \tau_h^C) \end{cases} \quad (52)$$

An important feature of the proposed approach is that it is fully compatible with (MNA) solvers [45], as they are based on a circuit approach.

Equations (52) constitute a set of DDEs [20]. Depending on delays  $\tau_h^L$  and  $\tau_h^C$  and on the time step, the previous set of equations may take a very sparse form, thus allowing a strong CPU-time saving by using sparse solvers. However, electrically small structures can also be analyzed by the previous equations because  $\tau_h^L = \tau_h^C \cong \mathbf{0}$ , and in a matrix form, they are given by

$$\begin{bmatrix} -\mathbf{A} & -\tilde{\mathbf{R}}_L \\ \tilde{\mathbf{R}}_C^{-1} & -\mathbf{A}^T \end{bmatrix} \cdot \begin{bmatrix} \mathbf{v}(k) \\ \mathbf{i}_L(k) \end{bmatrix} = \begin{bmatrix} \mathbf{\Psi}(k - 1) + \mathbf{v}_S^{\text{ext}}(k) \\ \tilde{\mathbf{R}}_C^{-1} \mathbf{\Phi}(k - 1) + \mathbf{i}_S(k) \end{bmatrix}. \quad (53)$$

Such equations have the same structures as those of the standard PEEC method once time discretization is applied [51]. Furthermore, the enhanced models do not require any auxiliary quantity as the only unknowns are the currents flowing in branches connecting two nodes and the potential of each node to infinity. It is also worth noting that the PEEC equivalent circuit for a two-node-one-inductance model resembles the circuit obtained by means of the standard approach with the exception that resistances, inductances, and capacitances are substituted by current-controlled voltage sources (CCVSs); the resulting equivalent circuit is shown in Fig. 4, where  $i_L(l, k)$  denotes the inductive current flowing in branch  $l$  at time step  $k$ ; analogously,  $i_c(m, k)$  is the capacitive current leaving node  $m$  at time step  $k$ ; finally,  $\tilde{R}_L(l, :)$  and  $\tilde{R}_C(m, :)$  refer to the  $l$ th and  $m$ th rows of matrices  $\tilde{\mathbf{R}}_L$  and  $\tilde{\mathbf{R}}_C$ , respectively. It is also noteworthy that, as the equivalent circuit structure is preserved, the proposed macromodel is fully suited for inhomogeneous ideal [28] and dispersive dielectrics [18] models as their incorporation requires only adding excess capacitances in series to branches connecting couples of nodes.

1) *CPU-Time Analysis*: The presented enhanced rPEEC technique improves the modeling accuracy by taking the

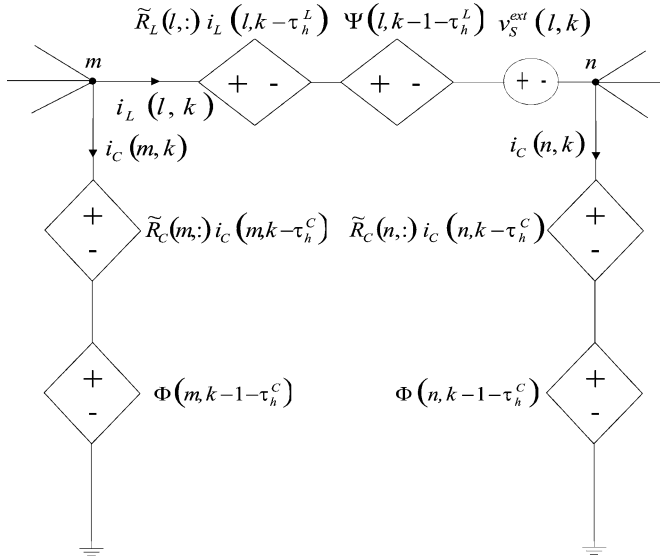
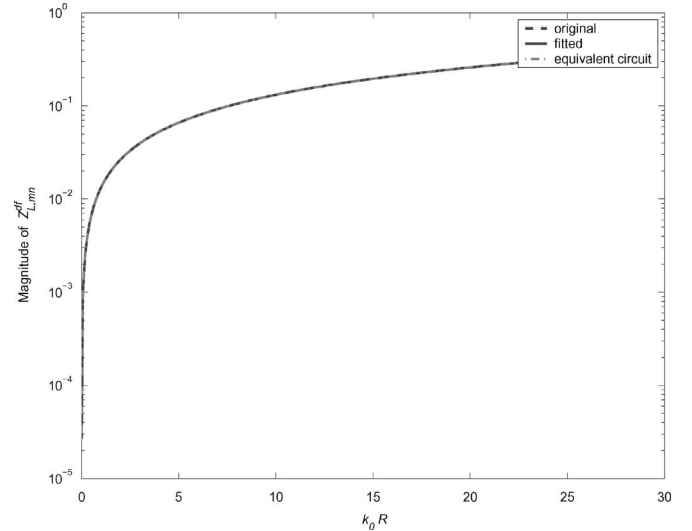
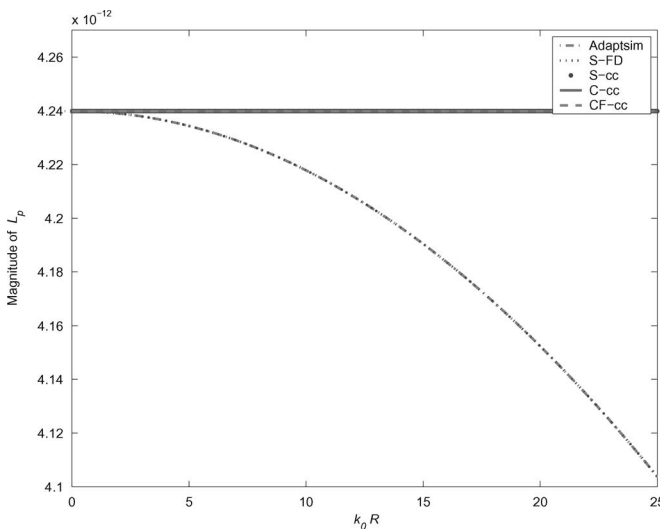


Fig. 4. Enhanced PEEC equivalent circuit.

Fig. 6. Magnitude spectrum of the pole-residue approximation of  $Z_{L,mn}^{d1}$  (Section VII-A).Fig. 5. Magnitude spectrum of the mutual partial inductance  $L_{p,mn}$  as a function of  $k_0 R$  (Section VII-A).

damping of the coupling into account at high frequencies. Accurately modeling the damping also improves the stability of the PEEC models. However, improvements require some additional computations: 1) The coupling coefficients (partial inductances and coefficients of potential) need to be computed over a wide frequency range, and 2) a rational model needs to be extracted. Both steps depend on setting parameters, which are as follows:

- order of numerical integration of double folded integration for partial element computation;
- number of frequency samples  $nf$ ;
- number of poles  $np$  used in the rational macromodel;
- number of iteration  $iter$  in the fitting procedure.

A typical setting is order = 10,  $nf = 40$ ,  $np = 3$ , and  $iter = 3$ . There is no doubt that the most time-consuming step is represented by the frequency sweep to generate the data to be

TABLE I  
RATIO OF CPU TIME FOR PARTIAL ELEMENT MATRICES FILL-IN  
AND CIRCUIT SYNTHESIS

	$L_P$	$P$	$Z_L^{dt}$	$Z_C^{dt}$
cpu-time ratio	100	90	1	1

fitted. The extraction of rational model (using OVF) takes less than 10% of the CPU time required to perform a single frequency sample computation. This means that the CPU time ratio scales, for each coupling coefficient, as the number of frequency samples.

It is worth mentioning that the rational macromodeling process can be significantly accelerated by means of advanced techniques such as adaptive frequency sampling (AFS) [52]. Moreover, a significant CPU time saving can be achieved by using multiple moments in the OVF procedure, allowing reduction of the number of frequency samples needed to obtain a user-defined maximum rms error. The combination of the two techniques, which will be presented in forthcoming reports, is very promising as it provides a significant speedup, while preserving the accuracy.

## VII. NUMERICAL TESTS

### A. Mutual Coupling Between Two Identical Cells

In the first test, two identical elementary PEEC cells have been considered. The mutual partial inductance has been computed in the range 0–12.5 GHz by using different methods. Their dimensions are  $l = \lambda_{\min}/10$ ,  $w = \lambda_{\min}/10$ , and  $t = \lambda_{\min}/1000$ , where  $\lambda_{\min}$  is the minimum wavelength of interest. The two cells are  $4\lambda_{\min}$  apart from each other.

The reference result has been obtained by an adaptive quadrature scheme (Adaptism) proposed by Gander and Gautschi [29]; next, a frequency-dependent Gauss–Legendre integration of order six over the surface (S-FD) has been used; then, the

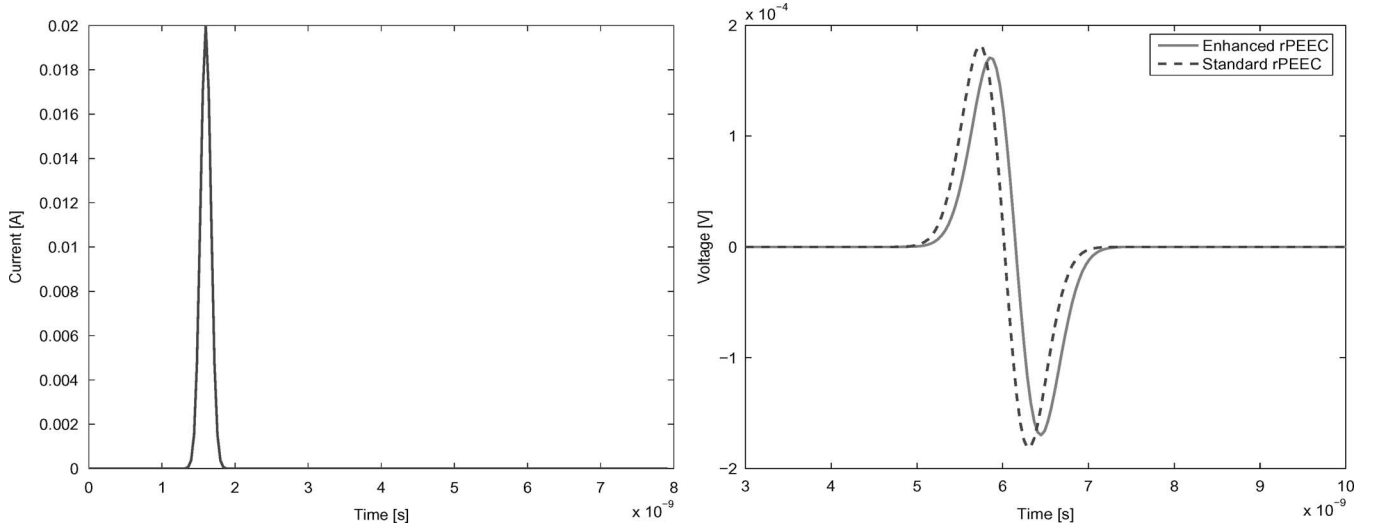
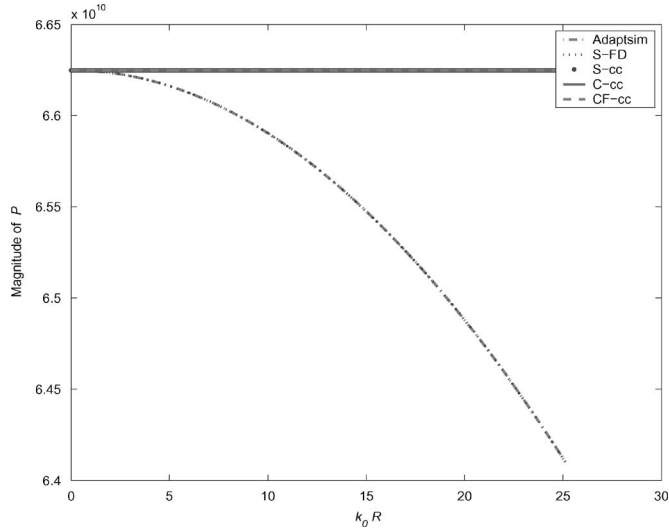
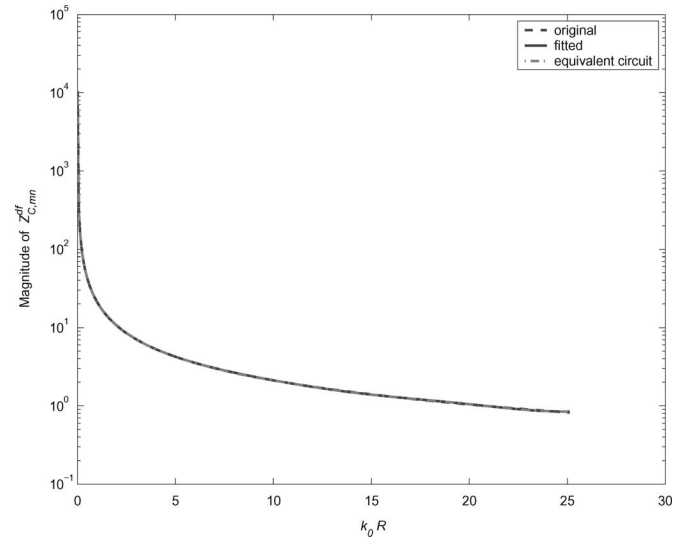


Fig. 7. Injected current and induced voltage in the far field case (Section VII-A).


 Fig. 8. Magnitude spectrum of the mutual coefficient of potential  $P_{mn}$  as a function of  $k_0 R$  (Section VII-A).

 Fig. 9. Magnitude spectrum of the pole-residue approximation of  $Z_{C,mn}^{dl}$  (Section VII-A).

center-to-center approximation has also been assumed, and the integral has been computed by using a frequency-independent surface integration (S-cc) and a contour integration (C-cc) [53]; finally, a closed formula [54] has also been adopted (CF-cc) and used as a reference for the magnitude.

The magnitude frequency spectrum of the mutual partial inductance  $L_{p,mn}$  is shown in Fig. 5.

A significant difference is found in magnitude when the frequency dependence inside or outside of the integral is considered. The proposed enhanced rPEEC procedure has been applied by first extracting the center-to-center delay and then by fitting the delayless impedances. Fig. 6 shows the magnitude spectrum of  $Z_{L,mn}^{dl}$  by using five poles. At least eight poles would be required if delay extraction was not used.

A test in time domain was performed. An impulsive current was injected into  $Z_{L,mn}^{dl}$ , and the corresponding induced voltage was computed by using both the proposed approach and

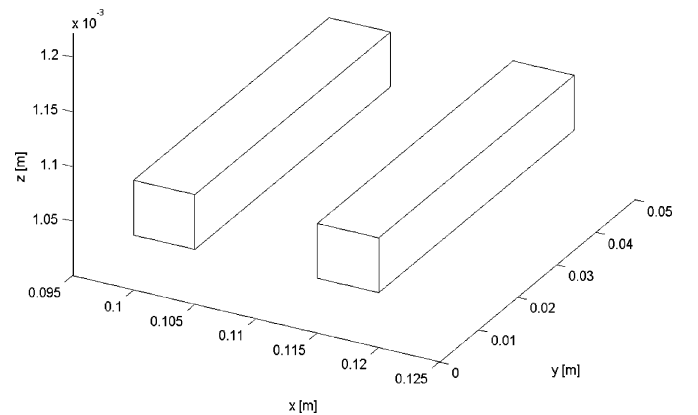


Fig. 10. Two-conductor transmission line.

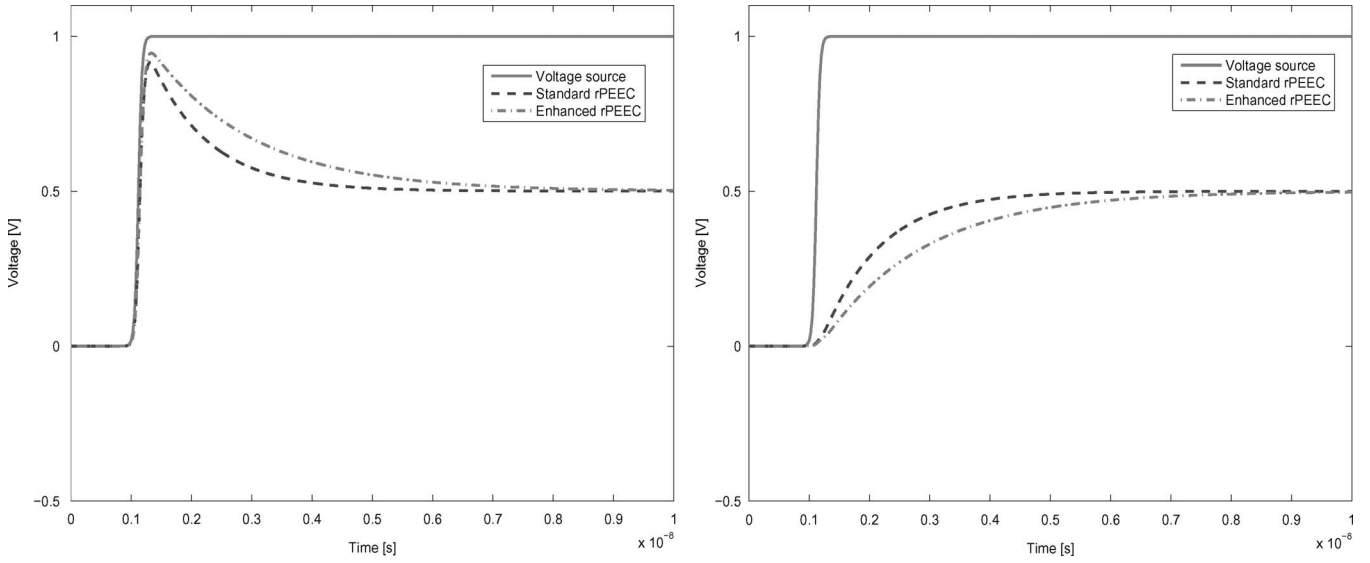


Fig. 11. Voltage source and port voltages (Section VII-B). (Left) Input port. (Right) Output port.

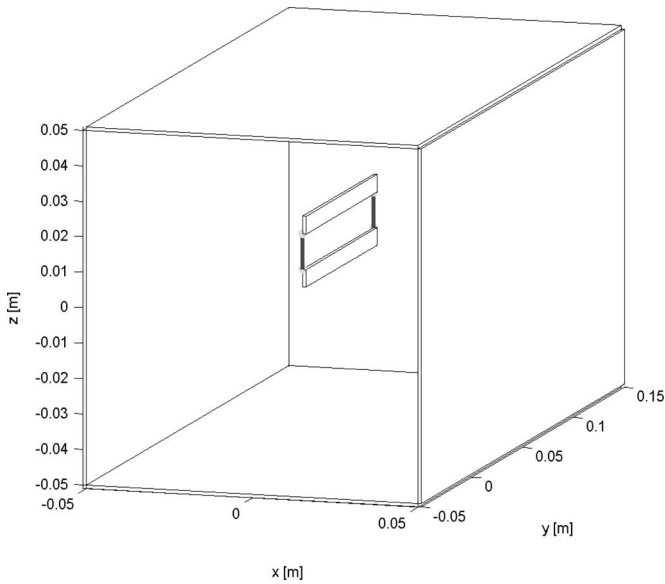


Fig. 12. Metallic enclosure and two-conductor transmission line.

the quasi-static approximation. Fig. 7 shows the comparison of voltages as computed by the proposed method and assuming the quasi-static hypothesis. In this case, the electrical distance at 5 GHz is  $k_0 R = 10$ , and thus, attenuation and dispersion are more pronounced. As expected and seen in Fig. 7, the enhanced model provides a larger attenuation and delay with respect to the standard approach. The larger electrical distance between coupled regions makes the frequency dependence of the mutual partial inductance stronger. As a consequence, a significant difference is found between the quasi-static and the enhanced solution.

The procedure has been repeated for the coefficient of potential as well. Fig. 8 shows the magnitude spectrum of  $P_{mn}$  as a function of  $k_0 R$ . In this case, the numerically computed delayless impedance  $Z_{C,mn}^d$  (original) has been fitted by using

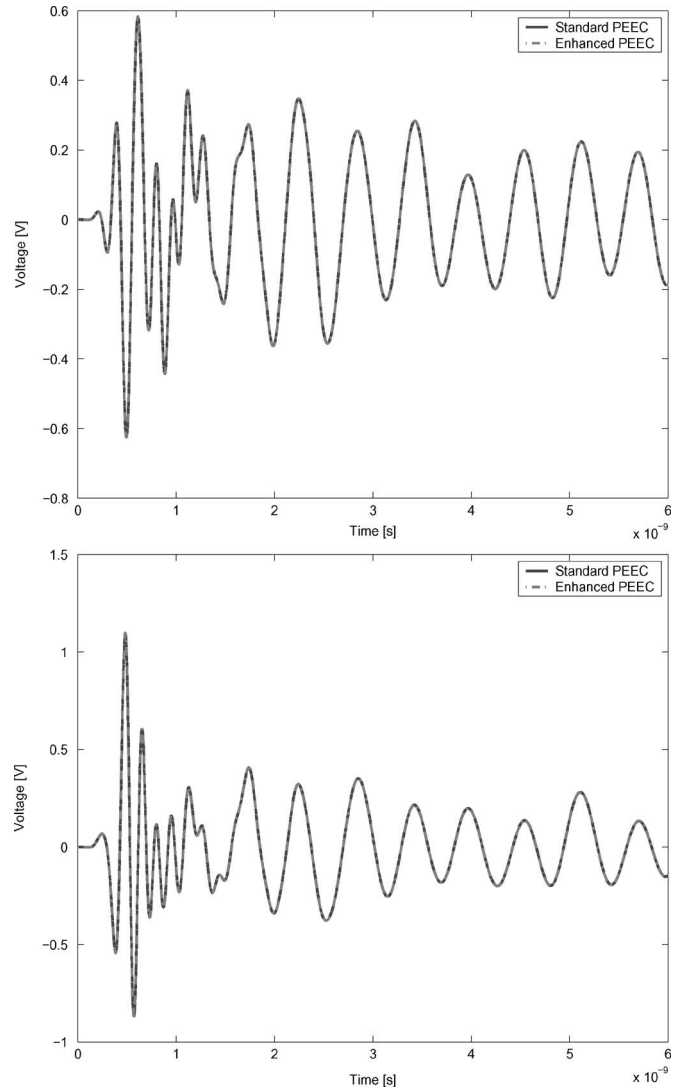


Fig. 13. Time domain voltage response (Section VII-C). (Top) Input port. (Bottom) Output port.

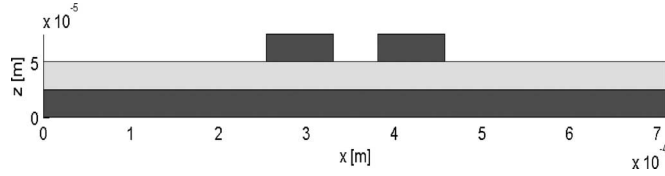


Fig. 14. Dimensions of the coplanar microstrip line.

five poles (fitted) and then synthesized into an equivalent circuit (equivalent circuit). The magnitude spectrum of  $Z_{C,mn}^{dl}$  is shown Fig. 9.

### B. Two-Conductor Transmission Line

As a second example, a two-conductor transmission line is shown in Fig. 10; the two conductors are 5 cm long and 0.5 cm apart. It has been modeled by PEEC using 216 inductive cells and 304 capacitive cells, resulting in 216 inductive currents  $i_L$  and 80 potentials  $v$  to infinity. The transmission line is terminated on 50- $\Omega$  resistances and driven by a voltage step whose frequency magnitude spectrum extends up to 10 GHz.

Table I reports the ratio of the CPU time required to fill in the matrices of partial elements  $L_P$  and  $P$  in the frequency range 0–20 GHz to that needed to perform the rational approximation and the circuit synthesis for all the impedances  $Z_L^{dl}$  and  $Z_C^{dl}$ .

The port voltages are computed by using both the standard PEEC and the enhanced models. The results are shown in Fig. 11 and confirm that additional losses due to frequency dependence of partial elements have a significant impact.

### C. Metallic Cabinet Enclosing a Transmission Line

In the following example, a two-conductor transmission line is placed at the center of a large metal enclosure that is open at one side, as sketched in Fig. 12. The conductors of the transmission line are 7 cm long, 0.5 cm thick, and 1.5 cm apart; they are terminated on 50- $\Omega$  resistances. The structure is excited by a plane wave that represents electromagnetic interference (EMI) due to an external electromagnetic source. The plane wave excitation is a modulated Gaussian pulse [55] defined by

$$\mathbf{E}^{\text{ext}}(\mathbf{r}, t) = \mathbf{E}_0 \cos \left[ 2\pi f_0 \left( t - t_p - \frac{\hat{\mathbf{k}} \cdot \mathbf{r}}{c} \right) \right] \times \exp \left[ -\frac{\left( t - t_p - \frac{\hat{\mathbf{k}} \cdot \mathbf{r}}{c} \right)^2}{2\sigma^2} \right]. \quad (54)$$

where

$$\mathbf{E}_0 = E_x \hat{\mathbf{x}} + E_y \hat{\mathbf{y}} + E_z \hat{\mathbf{z}}. \quad (55)$$

Assuming a spherical system of coordinates, the quantities in (55) are calculated using

$$\begin{aligned} E_x &= E_\theta \cos \theta_i \cos \phi_i - E_\phi \sin \phi_i \\ k_x &= \sin \theta_i \cos \phi_i \end{aligned}$$

$$\begin{aligned} E_y &= E_\theta \cos \theta_i \sin \phi_i + E_\phi \cos \phi_i \\ k_y &= \sin \theta_i \sin \phi_i \\ E_z &= -E_\theta \sin \theta_i \\ k_z &= \cos \theta_i. \end{aligned} \quad (56)$$

The other parameters in (54) are

$$\begin{aligned} f_0 &= 4\text{GHz} \\ \sigma &= \frac{1}{4\pi} \text{ns} \\ E_\theta &= -500\text{V/m} \\ \theta_i &= 135^\circ \\ t_p &= 0.5\text{ns} \\ E_\phi &= -500\text{V/m} \\ \phi_i &= 0^\circ \end{aligned} \quad (57)$$

which describe a modulated pulse propagating in the  $\hat{\mathbf{k}} = 0.7071\hat{\mathbf{x}} - 0.7071\hat{\mathbf{z}}$  direction. According to the MNA approach, inductive currents  $i_L$  and potentials to infinity  $v$  are assumed as unknowns; the number of unknowns for this geometry is  $N_L = 1056$  and  $N_C = 254$ . The computation of partial elements requires about 4 and 5 min for partial inductances and coefficients of potential, respectively. The time domain analysis has been simulated using a time step: over 3 ps (2000 time steps). On a 3.2-GHz AMD PC, this requires about 4 min of CPU time. The induced voltages on the terminal resistances obtained by the standard and the enhanced PEEC models are shown in Fig. 13.

In this case, excellent agreement is obtained between the standard and the enhanced PEEC models. Nonetheless, the enhanced model has superior stability property that ensures late time stability while the standard model fails to accomplish such a requirement.

### D. Coplanar Microstrip on a Dispersive and Lossy Dielectric Substrate

As a last example, a coplanar microstrip transmission line on a dispersive and lossy dielectric has been considered. Its geometry is illustrated in Fig. 14. The conductors are terminated on 50- $\Omega$  resistances, and one of them is driven by a 2-V pulse voltage source with 30-ps rise/fall time and 1-ns width. The time step is 10 ps. The dielectric substrate is constituted by DriClad. In the range of tens of gigahertz, it clearly exhibits a dispersive and lossy behavior, as confirmed by Fig. 15, which shows its permittivity and loss tangent  $\tan \delta$ , as obtained by using the method described in [56]. The incorporation of the lossy and dispersive dielectric has been accomplished by using the model described in [18]. The standard PEEC model clearly shows time instabilities that are already near the beginning of the time stepping process, while the enhanced PEEC model ensures stability as confirmed by Figs. 16 and 17, where the input and output port voltages are shown.

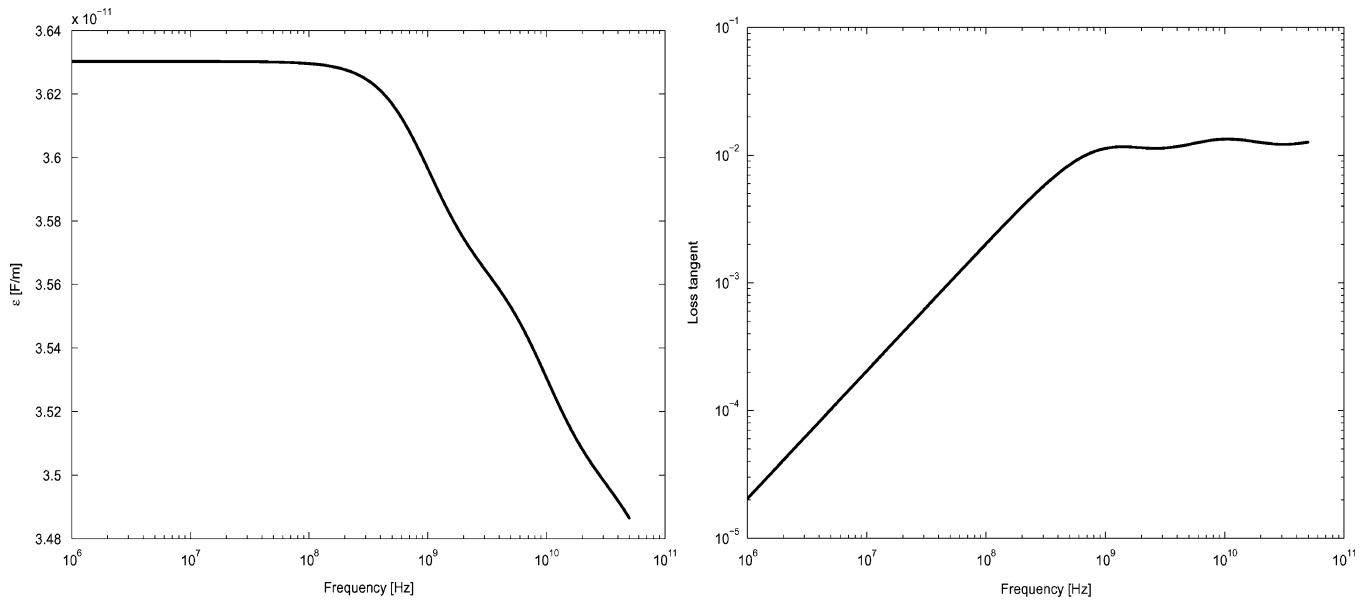


Fig. 15. DriClad substrate characteristics. (Left) Magnitude of permittivity. (Right) Loss tangent.

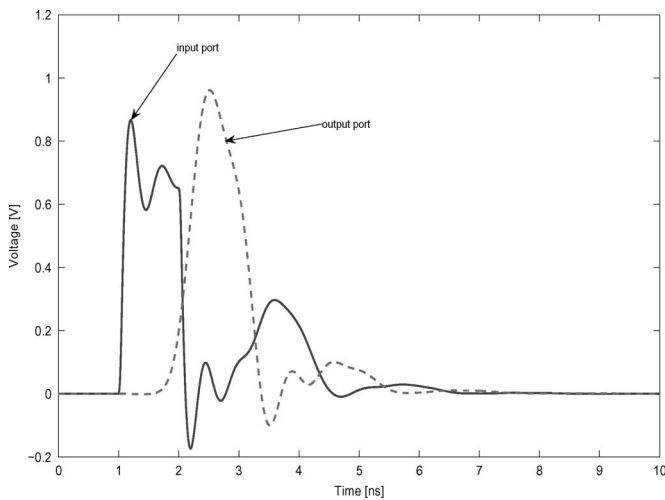


Fig. 16. Driven line port voltages (Section VII-D).

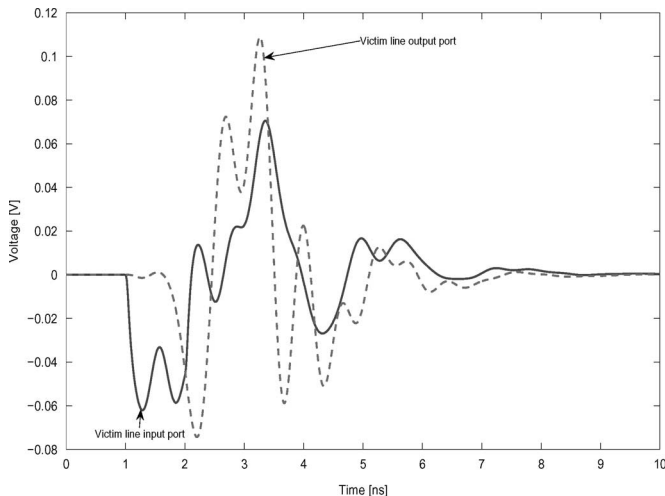


Fig. 17. Victim line port voltages (Section VII-D).

## VIII. CONCLUSION

In this paper, a new methodology is presented for taking into account the frequency dependence of PEEC partial elements, namely partial inductances and coefficients of potential, into a TD-PEEC solver. In the proposed methodology, frequency dependence of partial elements is exploited by using two techniques: 1) delay extraction and 2) rational approximation based on OVF. The former is analog to the one performed into standard PEEC models, and the latter allows to incorporate the damping of partial elements with increasing frequencies. The additional workload required by the second technique is limited due to the first technique. This results in the generation of time discrete PEEC macromodels that share the same elementary topology as the standard model but also include the frequency dependence of partial elements. Next, the enhanced models have been synthesized into equivalent circuits that are easily incorporated into a TD-PEEC solver based on MNA. The numerical tests presented have proven the robustness and accuracy of the proposed method in capturing the dispersive behavior of partial elements. Furthermore, as expected, the proposed technique significantly improves the stability properties of PEEC models. This will be investigated more in depth in future work. In order to speed up the computation of partial elements in the frequency domain, an AFS approach will be studied and reported as well.

As the development of TD-PEEC solvers continues, the ability of carefully modeling high-frequency effects is expected to play an increasingly important role in modeling larger and more complex systems in signal integrity and electromagnetic compatibility areas.

## REFERENCES

- [1] W. C. Chew *et al.*, "Fast solution methods in electromagnetics," *IEEE Trans. Antennas Propag.*, vol. 45, no. 3, pp. 533–543, Mar. 1997.
- [2] K. S. Yee, "Numerical solution of initial boundary value problems involving Maxwell's equations in isotropic media," *IEEE Trans. Antennas Propag.*, vol. AP-14, no. 5, pp. 302–307, May 1966.

- [3] A. Taflov and S. C. Hagness, *Computational Electrodynamics*. Norwood, MA: Artech House, 2000.
- [4] J. M. Jin, *The Finite Element Method in Electromagnetics*, 2nd ed. New York: Wiley, 2002.
- [5] W. C. Chew, J.-M. Jin, E. Michielssen, and J. Song, *Fast and Efficient Algorithms in Computational Electromagnetics*. Norwood, MA: Artech House, 2001.
- [6] L. Greengard, *The Rapid Evaluation of Potential Fields in Particle Systems*. Cambridge, MA: MIT Press, 1988.
- [7] J. M. Song and W. C. Chew, "Multilevel fast-multipole algorithm for solving combined field integral equations of electromagnetic scattering," *Microw. Opt. Technol. Lett.*, vol. 10, pp. 14–19, 1995.
- [8] A. A. Ergin, B. Shanker, and E. Michielssen, "The plane wave time domain algorithm for the fast analysis of transient wave phenomena," *IEEE Trans. Antennas Propag.*, vol. 41, no. 8, pp. 39–52, Aug. 1999.
- [9] B. Shanker, A. A. Ergin, K. Aygun, and E. Michielssen, "Analysis of transient electromagnetic scattering from closed surfaces using a combined field integral equation," *IEEE Trans. Antennas Propag.*, vol. 48, no. 7, pp. 1064–1074, Jun. 2000.
- [10] K. Aygün, B. Shanker, A. Ergin, and E. Michielssen, "A two-level plane wave time-domain algorithm for fast analysis of EMC/EMI problems," *IEEE Trans. Electromagn. Compat.*, vol. 44, no. 1, pp. 152–163, Feb. 2002.
- [11] A. Yilmaz, D. S. Weile, E. Michielssen, and J.-M. Jin, "A hierarchical FFT algorithm (HIL-FFT) for the fast analysis of transient electromagnetic scattering phenomena," *IEEE Trans. Antennas Propag.*, vol. 50, no. 7, pp. 971–982, Jul. 2002.
- [12] V. I. Okhmatowski, J. D. Morsey, and A. Cangellaris, "Loop-tree implementation of the adaptive integral method (AIM) for numerically-tractable, broadband, fast electromagnetic modeling," *IEEE Trans. Antennas Propag.*, vol. 52, no. 8, pp. 2130–2140, Aug. 2004.
- [13] A. E. Ruehli, "Equivalent circuit models for three dimensional multiconductor systems," *IEEE Trans. Microw. Theory Tech.*, vol. MTT-22, no. 3, pp. 216–221, Mar. 1974.
- [14] H. Heeb and A. Ruehli, "Three-dimensional interconnect analysis using partial element equivalent circuits," *IEEE Trans. Circuits Syst.*, vol. 38, no. 11, pp. 974–981, Nov. 1992.
- [15] A. Ruehli and H. Heeb, "Circuit models for three-dimensional geometries including dielectrics," *IEEE Trans. Microw. Theory Tech.*, vol. 40, no. 7, pp. 1507–1516, Jul. 1992.
- [16] A. E. Ruehli, G. Antonini, J. Esch, J. Ekman, A. Mayo, and A. Orlandi, "Non-orthogonal PEEC formulation for time and frequency domain EM and circuit modeling," *IEEE Trans. Electromagn. Compat.*, vol. 45, no. 2, pp. 167–176, May 2003.
- [17] K. Coperich, A. Ruehli, and A. Cangellaris, "Enhanced skin effect for partial-element equivalent circuit (PEEC) models," *IEEE Trans. Microw. Theory Tech.*, vol. 48, no. 9, pp. 1435–1442, Sep. 2000.
- [18] G. Antonini, A. E. Ruehli, and A. Haridass, "Including dispersive dielectrics in PEEC models," in *Dig. Elect. Perform. Electron. Packag.*, Princeton, NJ, Oct. 2003, pp. 349–352.
- [19] J. S. Zhao and W. C. Chew, "Integral equation solution of Maxwell's equation from zero frequency to microwave frequencies," *IEEE Trans. Antennas Propag.*, vol. 48, no. 10, pp. 1635–1645, Oct. 2000.
- [20] A. Bellen, N. Guglielmi, and A. Ruehli, "Methods for linear systems of circuit delay differential equations of neutral type," *IEEE Trans. Circuits Syst.*, vol. 46, no. 1, pp. 212–216, Jan. 1999.
- [21] A. E. Ruehli, U. Miekkala, and H. Heeb, "Stability of discretized partial element equivalent EFIE circuit models," *IEEE Trans. Antennas Propag.*, vol. 43, no. 6, pp. 553–559, Jun. 1995.
- [22] S. V. Kochetov and G. Wollenberg, "Stability of full-wave PEEC models: Reason for instabilities and way for correction," presented at the Int. Zurich Symp. Electromagn. Compat., Zurich, Switzerland, Feb. 2005.
- [23] —, "Stable time domain PEEC solution for pulse excited interconnection structures," in *Proc. IEEE Int. Symp. Electromagn. Compat.*, Chicago, IL, Aug. 2005, pp. 911–916.
- [24] D. Deschrijver and T. Dhaene, "Rational modeling of spectral data using orthonormal vector fitting," in *Proc. 9th IEEE Workshop Signal Propagat. Interconnects*, May 2005, pp. 111–114.
- [25] T. Dhaene and D. Deschrijver, "Generalised vector fitting algorithm for macromodelling of passive electronic components," *Electron. Lett.*, vol. 41, no. 6, pp. 299–300, Mar. 2005.
- [26] J. Cullum, A. Ruehli, and T. Zhang, "Model reduction for PEEC models including retardation," in *Dig. Elect. Perform. Electron. Packag.*, vol. 7, West Point, NY, Oct. 1998, pp. 287–290.
- [27] —, "A method for reduced-order modeling and simulation of large interconnect circuits and its application to PEEC models with retardation," *IEEE Trans. Circuits Syst. II*, vol. 47, no. 4, pp. 261–373, Apr. 2000.
- [28] A. E. Ruehli and H. Heeb, "Circuit models for three-dimensional geometries including dielectrics," *IEEE Trans. Microw. Theory Tech.*, vol. 40, no. 7, pp. 1507–1516, Jul. 1992.
- [29] W. Gander and W. Gautschi, "Adaptive quadrature—Revisited," *BIT, Numer. Math.*, vol. 40, pp. 84–101, 2000.
- [30] C. Hoer and C. Love, "Exact inductance equations for rectangular conductors with applications to more complicated geometries," *J. Res. Natl. Bur. Stand. C. Eng. Instrum.*, vol. 69, no. C, pp. 127–137, 1965.
- [31] F. W. Grover, *Inductance Calculations: Working Formulas and Tables*. New York: Dover, 1962.
- [32] S. A. Teo, B. L. Ooi, S. T. Chew, and M. S. Leong, "A fast PEEC technique for full-wave parameters extraction of distributed elements," *IEEE Microw. Wireless Compon. Lett.*, vol. 11, no. 5, pp. 226–228, May 2001.
- [33] G. Antonini and A. E. Ruehli, "Fast multipole and multi-function PEEC methods," *IEEE Trans. Mobile Comput.*, vol. 2, no. 4, pp. 288–298, Oct.–Dec. 2003.
- [34] S. Grivet-Talocia, H.-M. Huang, A. E. Ruehli, F. Canavero, and I. M. Abe Elfadel, "Transient analysis of lossy transmission lines: An efficient approach based on the method of characteristics," *IEEE Trans. Adv. Packag.*, vol. 27, no. 1, pp. 45–56, Feb. 2004.
- [35] J. D. Jackson, *Classical Electrodynamics*. New York: Wiley, 1975.
- [36] J.-F. Mao and Z.-F. Li, "Analysis of the time response of multiconductor transmission lines with frequency-dependent losses by the method of convolution-characteristics," *IEEE Trans. Microw. Theory Tech.*, vol. 40, no. 4, pp. 637–644, Apr. 1992.
- [37] A. Dounavis, N. Nakhla, R. Achar, and M. Nakhla, "Delay extraction and passive macromodeling of lossy coupled transmission lines," in *Dig. Elect. Perform. Electron. Packag.*, Oct. 2003, pp. 251–254.
- [38] B. Gustavsen and A. Semlyen, "Rational approximation of frequency domain responses by vector fitting," *IEEE Trans. Power App. Syst.*, vol. 14, no. 3, pp. 1052–1061, Jul. 1999.
- [39] B. Gustavsen, "Computer code for rational approximation of frequency dependent admittance matrix," *IEEE Trans. Power Del.*, vol. 17, no. 4, pp. 97–104, Oct. 2002.
- [40] D. Deschrijver and T. Dhaene, "Broadband macromodelling of passive components using orthonormal vector fitting," *Electron. Lett.*, vol. 41, no. 21, pp. 1160–1161, Oct. 2005.
- [41] E. C. Levi, "Complex curve fitting," *IRE Trans. Autom. Control*, vol. AC-4, pp. 37–44, 1959.
- [42] D. Deschrijver and T. Dhaene, "Parametric identification of frequency domain systems using orthonormal rational bases," in *Proc. 14th IFAC Symp. Syst. Identif.*, 2006, pp. 837–842.
- [43] S. Grivet-Talocia, "Enforcing passivity by perturbation of Hamiltonian matrix," *IEEE Trans. Circuits Syst.*, vol. 51, no. 9, pp. 1755–1769, Feb. 2004.
- [44] B. Gustavsen, "Enforcing passivity for admittance matrices approximated by rational functions," *IEEE Trans. Power Del.*, vol. 16, no. 1, pp. 97–104, Feb. 2001.
- [45] C. Ho, A. Ruehli, and P. Brennan, "The modified nodal approach to network analysis," *IEEE Trans. Circuits Syst.*, vol. CAS-22, no. 6, pp. 504–509, Jun. 1975.
- [46] G. Antonini, "SPICE compatible equivalent circuits of rational approximation of frequency domain responses," *IEEE Trans. Electromagn. Compat.*, vol. 45, no. 3, pp. 502–512, Aug. 2003.
- [47] J. Garrett, A. E. Ruehli, and C. R. Paul, "Accuracy and stability improvements of integral equation models using the partial element equivalent circuit PEEC approach," *IEEE Trans. Antennas Propag.*, vol. 46, no. 12, pp. 1824–1831, Dec. 1998.
- [48] J. E. Garrett and A. Ruehli, "PEEC-EFIE for modeling 3D geometries with lossy inhomogeneous dielectrics and incident fields," IBM T. J. Watson Research Center, Yorktown Heights, NY, IBM Res. Rep. RC 19245 (#83733), Oct. 1993.
- [49] L. Pillegi, R. Rohrer, and C. Visweswariah, *Electronic Circuits and System Simulation Methods*. New York: McGraw-Hill, 1995.
- [50] J. Ekman, G. Antonini, and A. Orlandi, "3-D PEEC capacitance calculation," in *Proc. IEEE Int. Symp. Electromagn. Compat.*, Boston, MA, Aug. 2003, pp. 630–635.
- [51] G. Antonini, "The fast multipole method for PEEC circuits analysis," in *Proc. IEEE Int. Symp. Electromagn. Compat.*, Minneapolis, MN, Aug. 2002, pp. 446–451.

- [52] T. Dhaene, J. Ureel, N. Faché, and D. De Zutter, "Adaptive frequency sampling algorithm for fast and accurate S-parameter modeling of general planar structures," in *Proc. IEEE Int. Microw. Symp.*, Orlando, FL, 1995, pp. 1427–1430.
- [53] G. Antonini, A. Orlandi, and A. Ruehli, "Analytical integration of quasi-static potential integrals on non-orthogonal coplanar quadrilaterals for the PEEC method," *IEEE Trans. Electromagn. Compat.*, vol. 44, no. 2, pp. 399–403, May 2002.
- [54] A. E. Ruehli, "Inductance calculations in a complex integrated circuit environment," *IBM J. Res. Dev.*, vol. 16, no. 5, pp. 470–481, Sep. 1972.
- [55] K. Aygün, B. Fischer, J. Meng, B. Shanker, and E. Michielssen, "A fast hybrid field-circuit simulator for transient analysis of microwave circuits," *IEEE Trans. Microw. Theory Tech.*, vol. 52, no. 2, pp. 573–583, Feb. 2004.
- [56] A. E. Engin, W. Mathis, W. John, G. Sommer, and H. Reichl, "Time domain modeling of lossy substrates with constant loss tangent," in *Proc. 6th IEEE Workshop Signal Propag. Interconnects*, Heidelberg, Germany, May 2004, pp. 151–154.



**Giulio Antonini** (M'94) received the Laurea degree (*summa cum laude*) from the University of L'Aquila, L'Aquila, Italy, in 1994 and the Ph.D. degree from the University of Rome "La Sapienza," Rome, Italy, in 1998, both in electrical engineering.

Since 1998, he has been with the Electromagnetic Compatibility Research Laboratory, Department of Electrical Engineering, University of L'Aquila, where he is currently an Associate Professor. He has collaborated with the IBM T. J. Watson Research Center, Yorktown Heights, NY, in the

development of algorithms for partial element equivalent circuit (PEEC) modeling. His current research interests include electromagnetic compatibility (EMC) analysis, numerical modeling, and the field of signal integrity for high-speed digital systems. He is the author or coauthor of more than 100 technical papers and has given nine keynote lectures at international conferences. He is the holder of a European patent. He is a Reviewer for a number of IEEE journals.

Prof. Antonini received the IEEE TRANSACTIONS ON ELECTROMAGNETIC COMPATIBILITY Best Paper Award in 1997, the CST University Publication Award in 2004, the IBM Shared University Research Award in 2004, 2005, and 2006, and a Technical Achievement Award from the IEEE EMC Society for innovative contributions to computational electromagnetic on the PEEC technique for EMC applications. He is a member of the TC-9 Committee and the Secretary of the TC-10 Committee of the IEEE EMC Society. He is a member of Technical Program Committee of the Date Conference.

**Dirk Deschrijver** was born in Tiel, Belgium, in 1981. He received the Master's degree in computer science in 2003 from the University of Antwerp, Antwerp, Belgium, where he is currently working toward the Ph.D. degree in computer science with the Computer Modeling and Simulation (COMS) research group, Department of Mathematics and Computer Science.

During May–October 2005, he was a Marie-Curie Fellow at Eindhoven University of Technology, Eindhoven, The Netherlands. His current research interests include least-squares rational approximation techniques, orthonormal rational functions, and frequency domain macromodeling.



**Tom Dhaene** (M'01–SM'06) was born in Deinze, Belgium, on June 25, 1966. He received the Ph.D. degree in electrotechnical engineering from the University of Ghent, Ghent, Belgium, in 1993.

From 1989 to 1993, he was a Research Assistant with the Department of Information Technology, University of Ghent, where he was engaged in different aspects of full-wave electromagnetic circuit modeling, transient simulation, and time-domain characterization of high-frequency and high-speed interconnections. In 1993, he joined the (EDA) company Alphabit (now part of Agilent). He was one of the key developers of the planar electromagnetic (EM) simulator advanced design system (ADS) momentum and is the principal developer of the multivariate EM-based adaptive metamodeling tool ADS Model Composer. Since September 2000, he has been a Professor with the Computer Modeling and Simulation (COMS) Group, Department of Mathematics and Computer Science, University of Antwerp, Antwerp, Belgium. He has developed a modeling and simulation EDA software. He is the author or coauthor of more than 100 peer-reviewed papers and abstracts in international conference proceedings, journals, and books. He is the holder of two U.S. patents.